Journal of Catalysis **203,** 477–486 (2001)
doi:10.1006/jcat.2001.3342, available online at http://www.idealibrary.com on IDEAL®

Mechanistic Study of Partial Oxidation of Methane to Synthesis Gas over Modified Ru/TiO_2 Catalyst

Costas Elmasides and Xenophon E. Verykios[1]

Department of Chemical Engineering, University of Patras, GR-26500 Patras, Greece

Received April 11, 2001; revised July 9, 2001; accepted July 16, 2001

The mechanism of the partial oxidation of methane to synthesis gas over the $Ru/TiO_2(Ca^{2+})$ catalyst is investigated employing non-steady-state and steady-state isotopic transient experiments, combined with *in situ* DRIFT spectroscopy. The main objective is to identify the active intermediate species involved in surface transformations and the mechanistic reaction pathways. It was found that gas-phase CH_4 interacts with the catalyst surface, producing CH_x surface species. This process is irreversible and is characterized by a slow rate. CH_x species are fully dehydrogenated toward surface carbon. Adjacent metallic Ru sites as well as atomically adsorbed oxygen participate in the process of hydrogen abstraction from CH_x species. The primary product of the reaction is CO, which results from the surface reaction between carbon and adsorbed atomic oxygen on metallic Ru sites, while CO_2 derives from CO oxidation on oxidized sites. The unique ability of the Ru/TiO_2 catalyst to promote the direct formation of H_2 and CO is attributed to its high resistance to oxidation under conditions of partial oxidation of methane.

1. INTRODUCTION

The catalytic partial oxidation of methane to synthesis gas has received significant attention in recent years because it may offer advantages over steam reforming, which is currently practiced in industry (1). Depending on the catalyst employed, two alternative reaction pathways have been proposed: (a) an "indirect" scheme, according to which the initial combustion of methane is followed by reforming of the unconverted methane, with CO_2 and H_2O produced primarily, and (b) a "direct" scheme, according to which methane conversion to synthesis gas occurs without the intermediate production of CO_2 and H_2O. Most of the relevant studies reported in the literature show that partial oxidation of methane proceeds via the indirect reaction scheme (2, 3), which is characterized by a sharp temperature spike near the entrance of the catalyst bed, due to the combustion reaction, and essentially zero CO and H_2 selectivity at low methane conversion (<25%), or when oxygen is present in the reaction mixture.

Recent investigations in this laboratory (4–6) have demonstrated that, in contrast to other Group VIII metal catalysts, TiO_2-supported Ru exhibits unique catalytic behavior in the reaction of partial oxidation of methane by promoting the direct conversion scheme at relatively low temperatures. In particular, it has been found that, in the absence of mass and heat transfer resistances, high selectivity to synthesis gas (>65%) is obtained over Ru/TiO_2 catalysts in the low methane conversion range (oxygen conversion <100%), whereas small or zero selectivity to synthesis gas is observed over Ru catalysts supported on carriers other than TiO_2, or over other metal catalysts under the same conditions. It has also been found that doping of the TiO_2 carrier with cations (Ca^{2+}) of valence lower than that of the host cation (Ti^{4+}) promotes further the direct formation of synthesis gas and improves the activity of the Ru catalysts (6). This phenomenon has been attributed to the stabilization of the Ru crystallites in their metallic state, under reaction conditions.

In the present study, mechanistic aspects of the partial oxidation of methane to synthesis gas over Ru supported on Ca^{2+}-doped TiO_2, are investigated by FTIR and transient techniques. The primary objective is to identify surface transformations as well as their relative rate, to characterize the slow steps in the sequence, and to identify the most significant active surface species, in view of a better understanding of the reaction mechanism.

2. EXPERIMENTAL PROCEDURES

2.1. Catalyst Preparation

The TiO_2 carrier, doped with 0.95 at.% Ca^{2+} was prepared by the method of high-temperature diffusion of the dopant cation into the crystal matrix of titania. The parent TiO_2 carrier used in the present study was obtained from Degussa (P25) (specific surface area: 50 ± 2 m^2/g) and the precursor used for preparation of the Ca^{2+}-doped

[1] To whom correspondence should be addressed. Fax: +30-61-991 527. E-mail: verykios@chemeng.upatras.gr.

0021-9517/01 $35.00

carrier, CaO, was obtained from Alfa Products. To prepare the Ca^{2+}-doped TiO_2 carrier, weighed amounts of TiO_2 and CaO so as to yield 0.95 at.% Ca^{2+} were slurried with distilled water and thoroughly mixed. The water was evaporated under continuous stirring and the residue was dried at 383 K for 24 h. The dried material was then heated to 1173 K at a heating rate of 4 K/min. It was maintained at 1173 K for 5 h and then slowly cooled to room temperature. The specific surface area of the doped carrier was found to be 12 m^2/g and the crystal matrix was entirely transformed to the rutile form, as shown by XRD analysis.

Ruthenium, at a metal loading of 0.5 wt%, was dispersed on the doped carrier employing the incipient wetness impregnation method, using $Ru(NO)(NO_3)_3$ (Alfa Products) as the starting material. After preparation, the catalyst was reduced under H_2 flow at 573 K for 2 h, and then stored in sealed vials until further use. The catalyst was characterized in terms of its metal dispersion employing hydrogen chemisorption at room temperature. Metal dispersion was obtained by extrapolation of the linear part of the H_2 chemisorption isotherms to zero pressure. Based on the H_2 chemisorption results, the dispersion of Ru on the present catalyst is 50%.

2.2. *Transient Experiments*

The flow apparatus and reactor used for the transient experiments have been described in detail elsewhere (7). The gas composition at the reactor outlet was continuously monitored with an on-line mass spectrometer (Fisons, SXP Elite 300H) equipped with a fast-response inlet capillary system. Calibration of the mass spectrometer signal was performed based on prepared mixtures of known composition. For all transient experiments, gas-phase composition was calculated from the MS signal at the following m/e ratios: 40 (Ar), 15 (CH_4), 44 (CO_2), 28 (CO), 32 (O_2), 2 (H_2), 30 ($C^{18}O$), 46 ($C^{18}O^{16}O$), 48 ($C^{18}O_2$), 20 (CD_4). The fragmentation of the different species was calibrated and contributions from other than the indicated species were subtracted, as was the background level.

Transient experiments were performed by switching from a reaction mixture of $CH_4/O_2/He = 6/3/91$(total flow rate 250 ml min^{-1}) to He or to an equivalent mixture containing $^{18}O_2$ instead of $^{16}O_2$ or CD_4 instead of CH_4.

The reactor, where the transient experiments were carried out, was a quartz tube of outer diameter 6 mm. An enlargement of 8 mm at the central part of the tube contained the catalyst bed, which was supported by quartz wool. The quantity of catalyst used was 5 mg. The catalyst particle size was in the range 0.12–0.18 mm. A type K thermocouple enclosed in a quartz thermowell of 3-mm outer diameter was positioned inside the catalyst bed for accurate measurement of catalyst temperature.

2.3. *In Situ DRIFT Experiments*

A Nicolet 740 FTIR spectrometer equipped with a DRIFT cell, an MCT detector, and a KBr beamsplitter was used in the present study. For all spectra, a 64-scan data acquisition was carried out at a resolution of 4.0 cm^{-1}. Samples examined were in finely powdered form and their surface was carefully flattened to increase the intensity of the IR beam by reflection. The apparatus and procedures for obtaining *in situ* FTIR spectra have been described in detail elsewhere (8).

In situ FTIR spectra were recorded under reaction conditions in the temperature range 773 to 1073 K. In these runs, each sample was first reduced in flowing hydrogen (20% H_2 in Ar) at 773 K for 60 min, and then the gas phase was purged by switching to Ar flow, at 773 K, for 10 min. After the purging process, the flow was switched to the reaction mixture and spectra were recorded after ca. 30 min on stream, when steady-state conditions had been achieved. Subsequently, the sample was heated at a higher reaction temperature under flow of the reaction mixture, and the next spectrum was recorded when the new reaction temperature had stabilized.

3. RESULTS

3.1. *Transient Experiments*

3.1.1. Steady-state isotopic transient experiment. The normalized transient responses obtained on switching, under steady-state conditions, from the reaction mixture $CH_4/^{16}O_2/He/Ar$ to the labeled mixture $CH_4/^{18}O_2/He$ at 923 K are presented in Fig. 1. Argon was used as an inert tracer. In this and in subsequent figures, breaks appear in

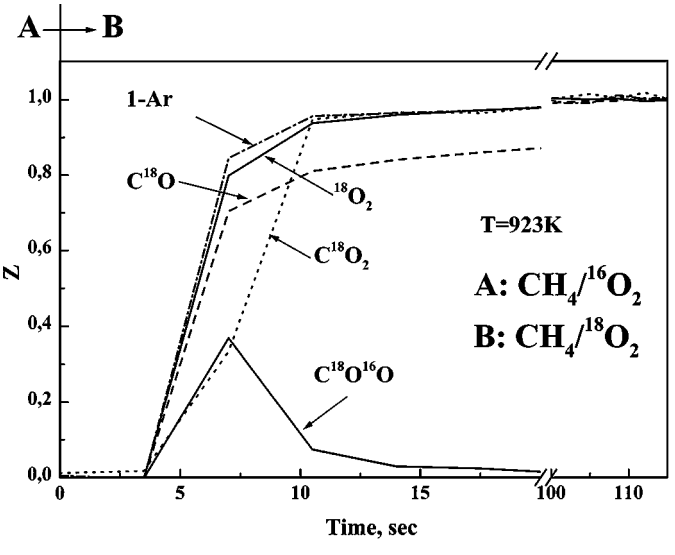

FIG. 1. Normalized responses of labeled species only, corresponding to the transient $CH_4/^{16}O_2/Ar/He$ (A) → $CH_4/^{18}O_2/He$ (B) at 923 K.

the response curves. This is due to the fact that a very large number of species (labeled and unlabelled) had to be monitored simultaneously, within very short time frames. As a result, the time resolution is not very good when rapid changes occur and some of the fine details are not apparent. The normalized responses of the labeled species only are shown in Fig. 1. Normalization is done on the basis of their steady-state composition, before and after the switch. More specifically, the results are expressed in terms of the variable Z, which is defined by the equation

$$Z(t) = (y(t) - y_0)/(y_\infty - y_0) \qquad [1]$$

where the subscripts 0 and ∞ refer to values of y (mole fraction) just before the switch ($t = 0$) and long after the switch ($t \to \infty$). Methane conversion and CO selectivity under steady-state conditions, before and after the switch, were 20 and 66%, respectively.

Figure 1 shows the normalized responses of $^{18}O_2$, $C^{18}O$, $C^{18}O_2$, and $C^{18}O^{16}O$ gas-phase species, which were observed on switching from the $CH_4/^{16}O_2$ to the $CH_4/^{18}O_2$ reaction mixture. The presence of $C^{18}O^{16}O$ at the outlet of the reactor, the signal of which appears simultaneously with that of $C^{18}O_2$ but reaches a maximum and decays quickly, points toward the interaction of surface species or adsorbed molecules originating from both reaction mixtures. More specifically, the gas-phase molecule $C^{18}O^{16}O$ is the product of the reaction between surface species $C^{18}O$–S and ^{16}O–S or $C^{16}O$–S and ^{18}O–S. This indicates that atomic oxygen or CO or both are accumulated on the catalyst surface under steady-state reaction conditions.

It should also be pointed out that the labeled molecule $C^{18}O_2$ is observed in the gas phase after $C^{18}O$. However, $C^{18}O_2$ production reaches steady state ($Z = 1$) faster than that of $C^{18}O$ (Fig. 1).

3.1.2. Non-steady-state transient kinetic experiment. Transient responses of reactant and products on switching from CH_4/O_2/He/Ar mixture to He at 923 K are presented in Fig. 2. It is observed that the response curves of CH_4, H_2, and CO follow closely that of the inert tracer, Ar, at least for the first 5 s after the switch. Such behavior suggests the weak and reversible adsorption of the corresponding molecules when the system operates under steady-state conditions. It must be noted that the curve of H_2 appears with a small delay after the initial 5 s. This delay is due to the fact that H_2 gas is produced by recombination of atomically adsorbed hydrogen, derived from the dehydrogenation of the weakly adsorbed CH_4. In contrast, a considerable delay is observed in the signal of CO_2. This implies that either CO_2 is strongly adsorbed or a surface reaction takes place during the transient period, which is responsible for its production. The latter is supported by the fast decay of O_2 with respect to the inert tracer, which could be explained by the participation of oxygen species in the surface reaction that

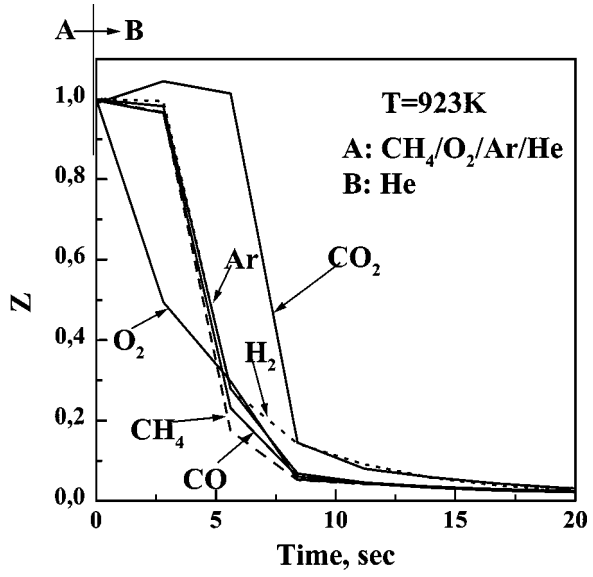

FIG. 2. Normalized responses after the transient CH_4/O_2/Ar/He → He at 923 K.

produces CO_2. This scheme implies the creation of new sites for oxygen adsorption and reaction during the transient period, which explain the fast decay of the oxygen signal. The CO, CO_2, and O_2 curves of Fig. 2 then point toward the existence of two kinds of adsorbed CO: one weakly and reversibly adsorbed, and one strongly adsorbed which is not desorbed but is oxidized to CO_2.

3.1.3. Kinetic isotope effect. A different kind of steady-state tracing experiment was performed to obtain kinetic information concerning the activation of methane, in particular to determine if the step(s) that involves C–H bond cleavage is slow. Thus, the kinetic isotopic influence of deuterium during the exchanges $CH_4/O_2 \to CD_4/O_2$ and $CD_4/O_2 \to CH_4/O_2$ at 903 K was studied. Figure 3a illustrates methane conversion and CO selectivity before and after the switch between the isotopic reaction mixtures. It is clear that during the exchange $CH_4/O_2 \to CD_4/O_2$, methane conversion as well as CO selectivity decreased, which implies the existence of kinetic isotopic influence in the reaction of partial oxidation of CH_4 over $Ru/TiO_2(Ca^{2+})$ catalyst. After the second exchange ($CD_4/O_2 \to CH_4/O_2$), while CO selectivity approximates its initial value (before the switch from CH_4/O_2 to CD_4/O_2), CH_4 conversion is stabilized at a somewhat lower level.

In Fig. 3b, the ratio of the steady-state rates of CH_4 consumption and CO and CO_2 production under conditions of CH_4/O_2 reaction, over the corresponding rates under conditions of CD_4/O_2 reaction, are shown. It is apparent that the deuterium-exchanged molecule results in significantly lower rates compared with normal methane. This rate reduction may be attributed to the kinetic isotopic influence. After steady state under CD_4/O_2 conditions was

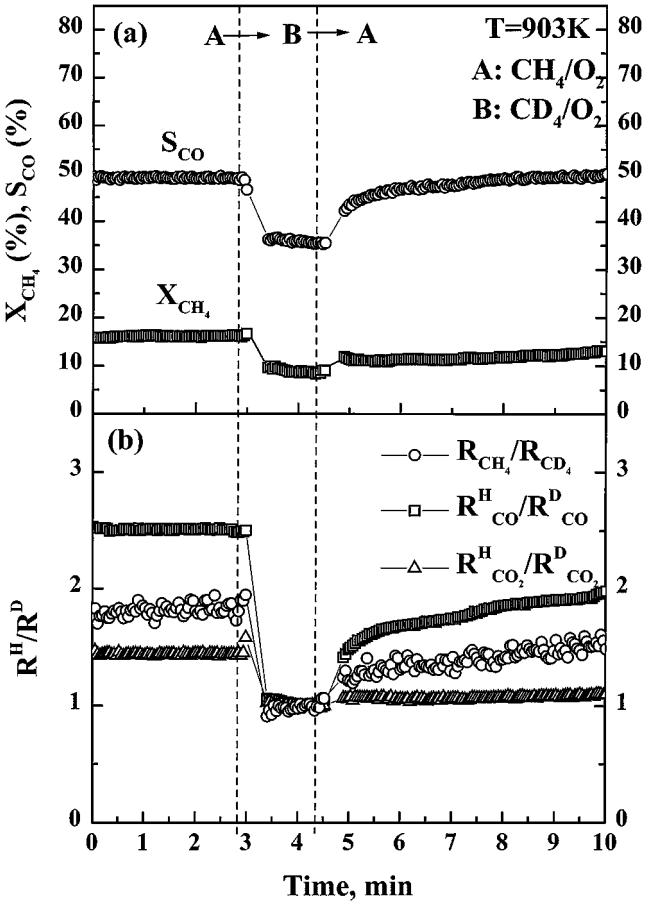

FIG. 3. Kinetic isotope effect during the exchanges $CH_4/O_2 \rightarrow CD_4/O_2 \rightarrow CH_4/O_2$ at 903 K, on (a) CH_4 conversion (X_{CH_4}) and CO selectivity (S_{CO}) and (b) the rates of CH_4 consumption and CO and CO_2 production.

established, a new switch to CH_4/O_2 reaction mixture (B → A) was performed. After the second exchange, an increase in CO formation and a modest increase in CH_4 consumption are observed, while the rate of CO_2 formation does not seem to be measurably influenced.

The fact that the original steady state is not achieved following the switch B → A implies that an alteration of the surface conditions has taken place on the switch A → B, and that the rate reduction, when the deuterium-containing molecule is used, may not be due exclusively to the kinetic isotope effect. In most probability, because the conversion of methane drops in the switch A → B, the temperature of the catalyst surface in state B is lower than that in state A. When the switch is reversed (B → A) the temperature at the catalyst surface is not sufficient to promote the system back to state A. Instead, a new state is observed in which the catalyst temperature is close to that of state B and the differences in rates are due to the kinetic isotope effect. Thus, the true kinetic isotope effect is manifested in the switch B → A, not in the switch A → B.

This concept was tested further by conducting a similar isotope exchange experiment at higher temperature (923 K) and the results are shown in Fig. 4. The results are qualitatively similar to those at the lower temperature (Fig. 3). However, in this case, the switch B → A is totally reversible since the same A state is achieved after the switch. This difference is due to the fact that, in the higher-temperature experiment, although the surface temperature dropped on the switch A → B, it still was at a sufficiently high level to be able to drive the system back to state A when the switch was reverted.

Based on these experiments, it is argued that safe conclusions concerning the possible kinetic isotopic influence can be derived only from the ratios R^H/R^D of the switch $CD_4/O_2 \rightarrow CH_4/O_2$ at 903 K, which is presented in Fig. 3. In similar types of experiments, especially when highly exothermic or highly endothermic reactions are involved, one must be careful to differentiate the role of surface temperature and its alteration with the various switches from possible kinetic isotopic influences.

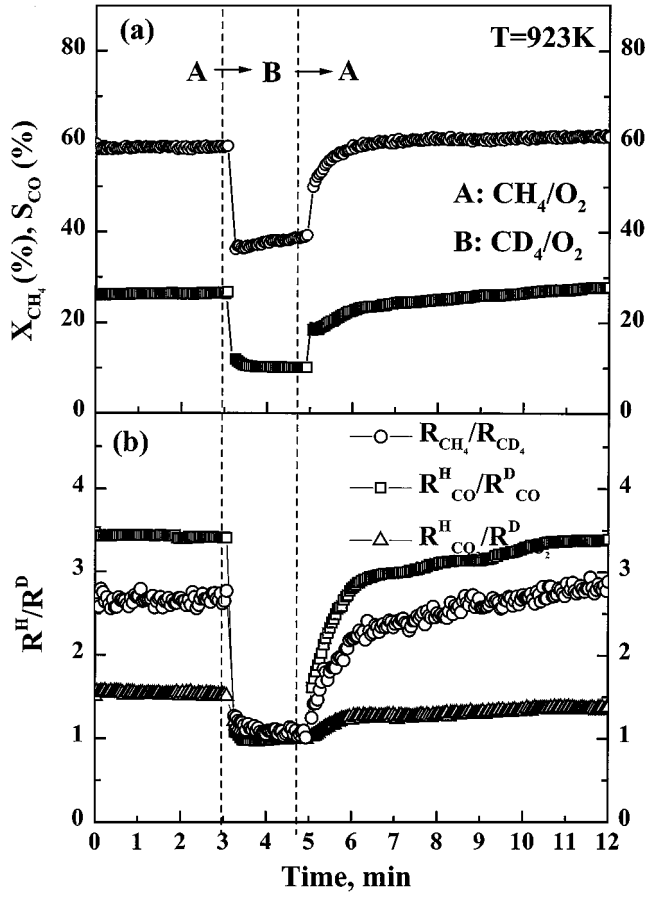

FIG. 4. Kinetic isotope effect during the exchanges $CH_4/O_2 \rightarrow CD_4/O_2 \rightarrow CH_4/O_2$ at 923 K, on (a) CH_4 conversion (X_{CH_4}) and CO selectivity (S_{CO}) and (b) the rates of CH_4 consumption and CO and CO_2 production.

TABLE 1

Kinetic Isotope Effect Following the Exchange $CD_4/O_2 \rightarrow CH_4/O_2$ at 903 K

	R^H/R^D		
	CH_4	CO	CO_2
Switch: $CD_4/O_2 \rightarrow CH_4/O_2$	1.6	1.9	1.02

The values of the R^H/R^D ratios for CH_4 consumption and CO and CO_2 production, following the switch B → A at 903 K, are summarized in Table 1. In the homogeneous dissociation of CH_4 (CD_4), the difference between the activation energies for the cleavage of C–H and C–D can be estimated as the negative value of the difference of their zero-point energies (18 kJ/mol for C–H and 13 kJ/mol for C–D (9)). This difference can be used to estimate the expected kinetic isotope effect (10). At 903 K, the calculated value of the kinetic isotope effect is 1.95; i.e., the rate of CH_4 dissociation is about twice that of CD_4. Hence, the experimental values of the R^H/R^D ratio in the case of CH_4 consumption and CO production are close to the theoretical ones. Furthermore, in the case of CO production, the experimental value of the R^H/R^D ratio is also close to the theoretical value of the O–H (O–D) bond, which is 2.1 at 903 K (11). On the contrary, there is no measurable change in the experimental value of the R^H/R^D ratio in the case of CO_2 production. Hence, the processes of CH_4 consumption and CO production are affected by the C–H cleavage of CH_4 and, consequently, are slow or rate-determining steps, while the opposite is true for CO_2 production. Furthermore, the above results clearly imply that CO production is directly related to adsorbed methane species, while CO_2 production is not.

3.2. *In Situ FTIR Spectra under Reaction Conditions*

In situ FTIR spectra obtained from $Ru/TiO_2(Ca^{2+})$ catalyst under reaction conditions, in the temperature range 773–1073 K, are presented in Fig. 5. In these experiments, the effluent from the IR cell was analyzed by gas chromatography and results concerning methane conversion and CO selectivity are summarized in Table 2. It is observed that interaction of the CH_4/O_2 mixture with the reduced catalyst at 773 K gives rise to FTIR bands due to gas-phase CH_4 (3250–2750 cm^{-1}), gas-phase CO_2 (2360/2340 cm^{-1}), surface hydroxyl groups (~3600 cm^{-1}), and a broadband at ca. 1995 cm^{-1}. Although bands due to gas-phase CO (2180/2100 cm^{-1}) are not present at this reaction temperature, analysis of the gas effluent at the exit of the FTIR cell shows that there was CO production (Table 2). The absence of the corresponding bands may be attributed to the relatively low concentration of CO in the gas phase.

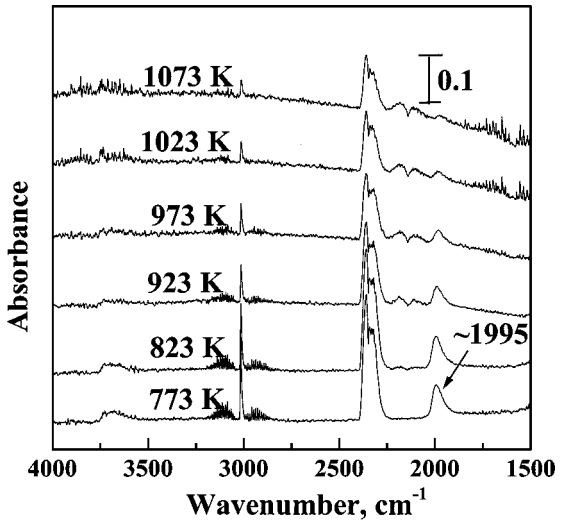

FIG. 5. *In situ* FTIR spectra obtained from $Ru/TiO_2(Ca^{2+})$ catalyst during interaction with a flowing 10% CH_4–5% O_2 (in Ar) mixture in the temperature range 773–1073 K.

Increasing reaction temperature to 823 K results in the appearance of bands due to gas-phase CO, located at around 2180 and 2100 cm^{-1}, which continuously increase in intensity with increasing temperature, up to 1073 K. At the same time, the bands due to gas-phase CO_2 and CH_4 decrease in intensity. This implies increased methane conversions and increased selectivities toward CO formation, which is confirmed by the GC analysis (Table 2). The 1995 cm^{-1} band also decreases in intensity with increasing reaction temperature but can be clearly observed at reaction temperatures as high as 1073 K. Analysis of this asymmetric broadband shows that it may be deconvoluted into two peaks located at ca. ~1995 and ~1955 cm^{-1} (Fig. 6). The position and relative intensity of these peaks, which will be denoted as "peak I" and "peak II," respectively, are listed in Table 3. While the position of peak II remains constant with increasing reaction temperature, the position of peak I remains constant up to 923 K and then shifts to lower frequencies (1985 cm^{-1}) with further increase in reaction temperature (Table 3). The relative intensity of peak I is slightly increased with increasing reaction temperature.

TABLE 2

Conversion of Methane (X_{CH_4}) and Selectivity toward CO (S_{CO}) Measured at the Exit of the FTIR Cell under the Conditions Described in Fig. 5

T_R (K)	X_{CH_4} (%)	S_{CO} (%)
773	16	8
823	26	36
973	36	64
1073	41	75

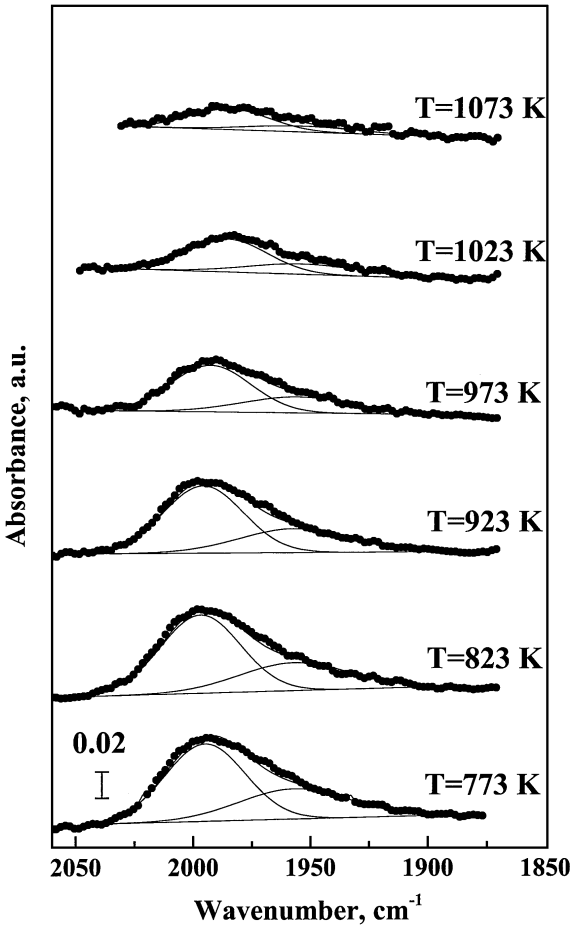

FIG. 6. Spectra of Fig. 5, expanded in the region 2050–1850 cm^{-1}.

In our previous study, bands observed in the region 2020–1950 cm^{-1} were attributed to CO species linearly bonded on metallic Ru clusters of low nuclearity and/or to clustered Ru^0 species in an ionic Ru^{n+} environment (8). However, these assignments were left open for further investigation.

TABLE 3

Spectral Parameters of Peaks I and II Obtained from the Deconvolution of the FTIR Spectra Presented in Fig. 6

	Peak position (cm^{-1})		
Temperature (K)	Peak I[a]	Peak II[b]	$I_I/(I_I + I_{II})$ (%)
773	1996	1955	65
823	1996	1955	67
923	1996	1955	67
973	1993	1955	68
1023	1986	1955	70
1073	1985	1955	71

[a] FWHM: 40 cm^{-1}.
[b] FWHM: 55 cm^{-1}.

In the present study, the origin of the bands observed at ca. 1995 cm^{-1}, which are the only bands due to adsorbed species present under reaction conditions, is discussed in more detail in the following section.

4. DISCUSSION

4.1. Origin and Nature of Surface Species Detected under Reaction Conditions

As shown in Fig. 5, the only IR bands observed under reaction conditions, which are attributable to adsorbed CO species, are those located at ~1995 cm^{-1} (species I) and ca. 1955 cm^{-1} (species II). These peaks appear at relatively low frequencies which indicates (a) very low surface coverage of the corresponding adsorbed CO species, and/or (b) adsorption on very small or isolated Ru sites, and/or (c) the presence of an electron donor in the vicinity of the adsorption sites.

Regarding the effect of surface coverage, it has been reported that adsorption of CO on Ru(001) single crystals results in the appearance of a single-frequency band, due to linearly bonded CO on reduced sites, shifting from 1984 to 2060 cm^{-1} with increasing CO coverage from 0.003 to 0.66 (12). Shifts of similar magnitude were observed by Kellner and Bell over Ru/Al_2O_3 catalysts (13). However, the highest and the lowest frequencies reported in that study were notably lower than those on single crystals, a result that was partly attributed to differences between the physical properties of alumina-supported Ru microcrystallites and bulk Ru metal (13). It is reasonable to assume that under the high-temperature reaction conditions employed in the present study, only low coverages of strongly adsorbed CO will be present on the catalyst surface.

The morphology and crystallite size of Ru may also influence the exact band position of adsorbed CO. Bands in the spectral region where peaks I and II are observed are characteristic of CO adsorbed on high index faces, where CO adsorbs more strongly than on a flat surfaces (14). This is supported by the fact that adsorption of CO on well-dispersed catalysts results in lower-frequency bands compared with the corresponding ones over sintered catalysts (14). As has been discussed in our previous study (8), spectral features located below 2020 cm^{-1} may be due to CO adsorbed on isolated Ru^0 entities of very low nuclearity and/or to Ru^0–CO species "diluted" in an oxidized environment.

The low frequency of peaks I and II may also be related to the presence of species like carbon and/or hydrogen in the vicinity of the adsorption sites. Solymosi *et al.* (15), who studied the interaction of $CO + H_2$ over supported Ru catalysts, observed an IR band at around 1990 cm^{-1} and attributed its relatively low absorption frequency to the formation of ruthenium carbonyl hydrides of the following

type:

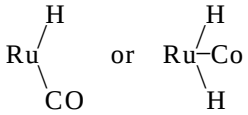

Similar were the findings of other investigators (16, 17) who studied the interaction of CO and $CO + H_2$ with supported Ru catalysts and observed bands very close to those observed in the present study. Based on the fact that these bands were observed on a freshly reduced surface, the authors attributed them to a Ru^0–CO-type linear species. Furthermore, they reported that the presence of hydrogen on the catalytic surface weakens the C–O bond of chemisorbed CO, resulting in a shift of the corresponding IR band toward lower frequencies. Hence, formation of ruthenium carbonyl hydrides produced through the dehydrogenation of methane could also explain the low vibrational frequencies observed in the present study (18):

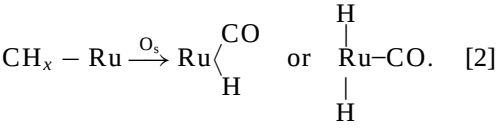

$$CH_4 + Ru \rightarrow CH_x - Ru \xrightarrow{O_s} Ru\langle^{CO}_{H} \quad \text{or} \quad \begin{matrix} H \\ | \\ Ru\text{–}CO. \\ | \\ H \end{matrix} \qquad [2]$$

Regarding the possible influence of surface carbon on the vibrational frequency of adsorbed CO species, it has been shown (16) that during hydrogenation of CO at high reaction temperatures, formation of carbon, originating from disproportionation of adsorbed CO, causes a further shift toward lower wavenumbers. Kellner and Bell (13) also assigned bands at frequencies as low as 1920 cm^{-1} to CO adsorbed in a linear mode to a Ru site adjacent to a nucleophilic adsorbate, such as carbon. This has been attributed to the property of carbon to act as an electron donor, thus enhancing the back-donation of electronic charge from the metal to the π^* orbitals of CO.

In the present case, surface carbon formed under reaction conditions could be responsible for the observed low frequencies of adsorbed CO species. If that is the case, one would expect to observe a shift of the band position toward lower frequencies with increasing concentration of surface carbon, especially at high CH_4 conversions ($X_{CH_4} > 35\%$), where oxygen is fully consumed and, therefore, carbon deposition is favored. A shift of ca. 10 cm^{-1} is observed with increasing temperature above 923 K (Table 3) where the CH_4 conversion is above 35% (Table 2). It should be noted that part of this shift could be attributed to the decrease in the surface coverage of this species, which takes place on increasing reaction temperature.

4.2. *Investigation of the Reaction Mechanism*

4.2.1. CH_4 activation. The transient response of CH_4 during the exchange from the CH_4/O_2 reaction mixture to He (Fig. 2) suggests that the interaction of CH_4 with the catalyst surface is a reversible process:

$$CH_4 + S \leftrightarrows CH_4 - S \quad (S[=] \text{ metallic surface active site}) \qquad [3]$$

The next step, after CH_4 adsorption on the catalyst surface, is the abstraction of atomic hydrogen and the creation of CH_x surface species. This process is irreversible. If it was not, then a delay of the CH_4 response with respect to the response of the inert tracer Ar (Fig. 2) would have been expected. Furthermore, the existence of kinetic isotope effect on the rate of CH_4 consumption indicates that this step is rate determining (rds).

Activation of CH_4 over metallic surface sites has been established in our previous work (6). More specifically, analysis of X-ray photoelectron spectra showed that the larger portion of Ru crystallites is in its metallic state under conditions of low CH_4 conversion, where gas-phase oxygen is not fully consumed (6).

4.2.2. CO and CO_2 production. There are two possible routes that the adsorbed surface species CH_x could follow: further dehydrogenation and creation of surface carbon and/or participation to a surface reaction toward CO and CO_2 formation:

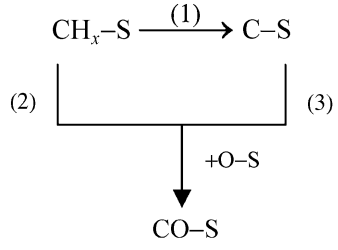

[4]

It is observed in Fig. 2 that the H_2 response appears with a slight delay with respect to that of Ar, after approximately 5 s from the exchange $CH_4/O_2 \rightarrow$ He. It is not clear whether this observation is real or an experimental artifact. If it is real it may be attributed to H_2 production, as a result of surface atomic hydrogen recombination. The only source of atomic hydrogen is the CH_x surface species,

$$CH_x\text{–}S + xS \rightarrow C\text{–}S + xH\text{–}S, \qquad [5]$$

$$2H\text{–}S \rightarrow H_2 + 2S, \qquad [6]$$

which survive on the catalyst surface even after removal of the CH_4/O_2 mixture from the gas phase. In our previous work, CH_x species on the catalyst surface under reaction conditions were detected by X-ray photoelectron spectroscopy [6]. Likewise, an indication of the existence of CH_x species on the catalyst surface may be derived from the stronger kinetic isotope effect in the case of CO production than CH_4 consumption (Table 1). This observation

implies that the production of adsorbed CO is strongly influenced by the interaction of CH_4 with the catalyst surface (Eqs. [3] and [5]) as well as the disruption of hydrogen bonds from the CH_x surface species:

$$\begin{aligned} &CH_x\text{–S} + S \rightarrow CH_{(x-1)}\text{–S} + H\text{–S} \\ &\vdots \\ &C\text{–S} + O\text{–S} \rightarrow CO\text{–S} + S \end{aligned} \qquad [7]$$

or

$$\begin{aligned} &CH_x\text{–S} + O\text{–S} \rightarrow CH_{(x-1)}\text{–S} + HO\text{–S} \\ &\vdots \\ &C\text{–S} + O\text{–S} \rightarrow CO\text{–S} + S \end{aligned} \qquad [8]$$

or

$$CH_x\text{–S} + O\text{–S} \rightarrow [CH_xO] \rightarrow CO\text{–S} + xH\text{–S} \qquad [9]$$

or

$$CH_x\text{–S} + HO\text{–S} \rightarrow [CH_xO] \rightarrow CO\text{–S} + xH\text{–S}. \qquad [10]$$

Obviously, one or more of the above elementary steps take place at slow rate. It must be emphasized that the reactions described by Eqs. [7]–[10] have been proposed in the literature of the catalytic partial oxidation of methane to synthesis gas formation (19–26). Moreover, Eq. [10] includes also the case in which $x = 0$. The sum of the reactions described by Eq. [10] ($0 \leq x < 4$) constitutes the basic surface elementary steps in the case of CH_4 reforming with steam (27).

It is apparent that many possible mechanistic pathways lead to the formation of surface adsorbed CO. The experimental observation that distinguishes two of the above four groups of elementary steps is the value of the R^H/R^D ratio for the case of CO production (Table 1). As already mentioned, this value is close to the theoretical value that arises from the difference between the energies in the zero level of the H–O and D–O bonds. Only the elementary surface transformations [8] and [10] involve surface OH species in the CH_4 dehydrogenation process which leads to the formation of adsorbed CO. The dominance of surface transformations [8] and the relatively high concentration of OH groups, which are the intermediate species for H_2O production, would justify the relatively low selectivity toward H_2 formation that the present catalyst exhibits (6). Although the group of reactions (7) does not include the formation of O–H bonds, the possibility that these surface elementary reactions do take place is not ruled out. It has been confirmed that under reaction conditions a large part of the catalyst surface is in its metallic state (6).

At this point, the behavior of the labeled molecule $C^{18}O$, after the exchange $CH_4/^{16}O_2/Ar/He \rightarrow CH_4/^{18}O_2/He$ (Fig. 1), deserves some comment: Although the $C^{18}O$ signal appears rapidly, almost simultaneously with that of O_2, it approaches steady state very slowly, after approximately 100 s. The isotopic tracing technique is based on the concept of steady-state conservation, as regards the concentrations of surface species, within the transition from the unlabeled to the labeled mixture. Consequently, the delay in the stabilization of a signal ($C^{18}O$ in the present case) could be attributed to the delay in the removal from the reactor of some other molecule that shares similar surface sites or surface intermediate species that participate in the formation of $C^{18}O$. The curves in Fig 1 indicate that there is no such molecule, among the molecules monitored, that may be responsible for the delay of $C^{18}O$ production to approach steady state. However, the responses of H_2, H_2O, and $H_2{}^{18}O$ have not been monitored. Important information could be obtained by the H_2O response, recording of which was not feasible because of condensation.

It has been reported in the literature that the surface reaction responsible for H_2O formation includes the interaction of atomically adsorbed hydrogen with hydroxyl surface groups (19, 21, 23, 26):

$$H\text{–S} + HO\text{–S} \rightarrow H_2O\text{–S} + S. \qquad [11]$$

It is obvious that surface OH groups are involved in H_2O production as well as in some other possible surface reactions concerning CH_4 dehydrogenation and CO production (Eqs. [8] and [10]). The existence of OH on the surface of the $Ru/TiO_2(Ca^{2+})$ catalyst under reaction conditions has been experimentally confirmed by IR spectroscopy (Fig. 5).

Assuming that after interruption of the $CH_4/^{16}O_2$ reaction mixture, strongly adsorbed hydroxyl groups containing ^{16}O will remain on the catalyst surface, then the production of $H_2{}^{16}O$ will continue according to Eq. [11]. Surface active sites are released by consumption of OH groups. Further dehydrogenation of CH_x species and/or oxygen adsorption take place on these active sites. The adsorbed oxygen assists in the process of hydrogen abstraction from CH_x species. This reasoning, coupled with the fact that there is no delay of $C^{16}O$ signal with respect to Ar in Fig. 1a, leads to the conclusion that the contribution of reactions group [10], toward CO production via the interaction of CH_x and OH species, is negligible.

The assumption of strongly adsorbed OH groups justifies the slow rate by which the R^H/R^D ratio, for CO production, approaches a constant value after the exchange $CD_4/O_2 \rightarrow CH_4/O_2$ (Fig. 3b). In this specific case, the responsible surface species are labeled hydroxyl groups, DO, which react with adsorbed atomic hydrogen and/or deuterium toward HDO and/or D_2O formation, respectively. Hence, the kinetic isotope effect for CO production becomes fairly complicated. However, the higher value of the kinetic isotope effect in the case of CO production is not in

question since it is present from the first seconds after the exchange $CD_4/O_2 \rightarrow CH_4/O_2$ (Fig. 3b).

The reactions in Eq. [9] include CH_xO as intermediate surface species. Considering the kinetic isotope effect, the formation or dissociation rate of CH_xO species should be slow. The formation of CH_xO ($x = 1, 2$) surface species and their dissociation toward surface CO constitute the surface elementary steps in the mechanism suggested by Xu and Froment (28) and Wang *et al.* (23), for the partial oxidation of methane over Rh/Al_2O_3 catalyst. In the former work, it was recommend that the production of surface CO from CH_xO surface species is a slow step and represents the rate-determining step of the CH_4 reforming reaction with H_2O over $Ni/MgAl_2O_4$ catalyst. Bradford and Vannice (29) used the same assumption to describe CH_4 reforming with CO_2 over TiO_2-supported metal (Cu, Rh, Pt, Pd, and Ni) catalysts. An adsorption band at 1690 ± 10 cm^{-1}, attributed to $H_2C{=}O$ surface species at the metal–support interface, was reported (29) in support of this assumption. In the present study, the absence of adsorption bands in this range, under reaction conditions (Fig. 5), implies that such intermediate surface species may not participate in the reaction mechanism. Hence, the kinetic isotope effect in the case of CO production may be attributed to other surface reaction pathways, in which formation or disruption of hydrogen bonds of surface species (Eq. [8]) takes place. Based on the discussion above, Eqs. [7] and/or [8] describe the possible mechanistic schemes responsible for CO production, while Eqs. [9] and [10] are excluded.

The delay of the CO_2 signal and the rapid decline of the O_2 signal (Fig. 2) were attributed to further oxidation of surface species. This was also confirmed by the transient response during the switch from $CH_4/^{16}O_2$ to $CH_4/^{18}O_2$ reaction mixture (Fig. 1). The delay in the appearance of $C^{18}O_2$ (Fig. 1), as well as the appearance of the labeled molecule $C^{18}O^{16}O$ (Fig. 1) prior to $C^{18}O_2$, implies that CO is the intermediate species responsible for CO_2 production:

$$\text{CO–S} + \text{O–S} \rightarrow \text{CO}_2\text{–S} + \text{S}. \qquad [12]$$

CO accumulation on the catalyst surface is revealed by the IR adsorption band at ~1995 cm^{-1} (Fig. 5). This band was attributed to adsorbed CO surface species. Also, CO accumulation could justify the value of the $R^{\mathrm{H}}/R^{\mathrm{D}}$ ratio for the rate of CO_2 production, which is approximately unity (Table 1). In other words, the rate of CO_2 production is independent of the rate of adsorbed CO production.

After the exchange $CH_4/^{16}O_2 \rightarrow CH_4/^{18}O_2$, the signal of $C^{18}O$ is observed very fast but it is stabilized after 100 s while the $C^{18}O_2$ signal is stabilized much faster. Additionally, CO selectivity at steady state was found to be of the order of 66%, indicating that CO oxidation is not favored. Analysis of the asymmetric broadband of the IR spectrum (~1995 cm^{-1}), which was attributed to adsorbed CO species, showed that it may be deconvoluted into two peaks located at ca. 1995 and 1955 cm^{-1} (Fig. 6). Hence, it may be assumed that peak I (2000–1980 cm^{-1}) corresponds to an adsorption site (S_1) where CO can accumulate without being oxidized and desorb, and peak II (ca 1955 cm^{-1}) corresponds to a different site (S_2) which favors further oxidation of CO to CO_2. This hypothesis is supported by the fact that the relative intensity of peak I (Table 3) increases with increasing reaction temperature, following the same trend with selectivity toward CO. Strong evidence of two types of adsorbed CO originates in a detailed kinetic study of the present catalytic system (30).

It could be further assumed that the dissociation of CH_4 and the production of CO (species I) take place on the same surface active sites S_1. This assumption is supported by the frequency shift of peak I when the conditions are favorable for carbon deposition (Fig. 6, Table 3). The absence of adsorbed oxygen on adjacent sites allows desorption of CO without its further oxidation to CO_2 on these sites.

Concerning the nature of the Ru sites where CO (species II) is adsorbed and oxidized toward CO_2, these sites must be either oxidized or "diluted" in an oxidizing environment. The latter is in accordance with the assignment of this band to monocarbonyl CO adsorbed at isolated Ru entities.

It was previously mentioned that the delay of $C^{18}O$ production to approach steady state (Fig. 1) is due to the corresponding delay of the consumption of adsorbed OH. In other words, there is no interaction between the surface species CO and OH. If the opposite were true, $C^{16}O^{18}O$ signal would appear with a similar delay in Fig. 1, due to the reaction

$$\text{C}^{18}\text{O–S} + \text{H}^{16}\text{O–S} \rightarrow \text{C}^{16}\text{O}^{18}\text{O–S} + \text{H–S}. \qquad [13]$$

The previous surface reaction [13] constitutes the basic elementary step in the mechanism of the water–gas shift reaction (23, 27). Since the results of the present study do not support the occurrence of the reaction [13], it may be deduced that the water–gas shift reaction does not take place over the Ru catalyst in the presence of oxygen in the gas phase.

5. CONCLUSIONS

The following conclusions may be drawn from the results of the mechanistic study of the partial oxidation of methane to synthesis gas over $Ru/TiO_2(Ca^{2+})$ catalyst:

- CH_4 dissociation takes place irreversibly toward CH_x surface species. This surface process is characterized by a slow rate and constitutes one of the steps that control the overall process.
- CH_x species are further dehydrogenated toward surface carbon (Eqs. [7] and [8]) and do not participate directly to CO formation via CH_x–O species (Eqs. [9] and [10]). In the process of hydrogen abstraction from CH_x species

participate adjacent metallic sites as well as atomically adsorbed oxygen.

- CO is the primary product of the reaction, which results from the surface reaction between carbon and adsorbed atomic oxygen (Eqs. [7] and [8]), while CO_2 derives from CO oxidation (Eq. [12]).
- There are at least two active surface sites under reaction conditions where the direct formation of synthesis gas is taking place. The larger part of the active surface is characterized by metallic Ru crystallites (S_1) where CH_4 adsorption and dissociation, carbon formation, and CO production take place and there is a small portion of the active surface (S_2) in which CO_2 is produced by combustion of CO.
- CH_4 reforming with H_2O and the water–gas shift reaction do not take place in the presence of gas-phase oxygen.

REFERENCES

1. Pena, M. A., Gomez, J. P., and Fierro, J. L. G., *Appl. Catal. A* **144**, 7 (1996).
2. Dissanayake, D., Rosynek, M. P., Kharas, K. C. C., and Lunsford, J. H., *J. Catal.* **132**, 117 (1991).
3. Dissanayake, D., Rosynek, M. P., and Lunsford, J. H., *J. Phys. Chem.* **97**, 3644 (1993).
4. Boucouvalas, Y., Zhang, Z. L., Efstathiou, A. M., and Verykios, X. E., *Stud. Surf. Sci. Catal.* **101**, 443 (1996).
5. Boucouvalas, Y., Zhang, Z. L., and Verykios, X. E., *Catal. Lett.* **40**, 189 (1996).
6. Elmasides, C., Kondarides, D. I., Neophytides, S. G., and Verykios, X. E., *J. Catal.* **198**, 195 (2001).
7. Efstathiou, A. M., and Verykios, X. E., *Appl. Catal. A* **151**, 109 (1997).
8. Elmasides, C., Kondarides, D. I., Gruenert, W., and Verykios, X. E., *J. Phys. Chem. B* **103**, 5227 (1999).
9. Drenth, W., and Kwart, H., "Kinetics Applied to Organic Reactions." Dekker, New York, 1980.
10. Laidler, K. J., "Reaction Kinetics," Vol. I: "Homogeneous Gas Reactions." Pergamon, London, 1963.
11. Au-Yeung, J., Chen, K., Bell, A., and Iglesia, E., *J. Catal.* **188**, 132 (1999).
12. Pfnur, H., Menzel, D., Hoffman, F., Ortega A., and Bradshaw, A. M., *Surf. Sci.* **93**, 431 (1980).
13. Kellner, C. S., and Bell, A. T., *J. Catal.* **71**, 296 (1981).
14. Guglielminotti, E., Spoto, G., and Zecchina, A., *Surf. Sci.* **161**, 202 (1985).
15. Solymosi, F., Tombacz, I., and Kocsis, M., *J. Catal.* **75**, 78 (1982).
16. Dalla Betta, R. A., and Shelef, M., *J. Catal.* **48**, 111 (1977).
17. Gupta, N. M., Kamble, V. S., Iyer, R. M., Ravindranathan Thampi, K., and Gratzel, M., *J. Catal.* **137**, 473 (1992).
18. Tian, Z., Dewaele, O., and Marin, G. B., *Catal. Lett.* **57**, 9 (1999).
19. Hickman, D. A., and Schmidt, L. D., *J. Catal.* **138**, 267 (1992).
20. Mallens, E. P. J., Hoebink, J. H. B. J., and Marin, G. B., *Catal. Lett.* **33**, 291 (1995).
21. Hu, Y. H., and Ruckenstein, E., *Catal. Lett.* **34**, 41 (1995).
22. Buyevskaya, O. V., Walter, K., Wolf, D., and Baerns, M., *Catal. Lett.* **38**, 81 (1996).
23. Wang, D., Dewaele, O., De Groote, A. M., and Froment, G. F., *J. Catal.* **159**, 418 (1996).
24. Au, C. T., and Wang, H. Y., *J. Catal.* **167**, 337 (1997).
25. Erdóhelyi, A., Fodor, K., and Solymosi, F., *J. Catal.* **166**, 244 (1997).
26. Fathi, M., Monnet, F., Schuurman, Y., Holmen, A., and Mirodatos, C., *J. Catal.* **190**, 439 (2000).
27. Alstrup, I., Clausen, B. S., Olsen, C., Smits, R. H. H., and Rostrup-Nielsen, J. R., *Stud. Surf. Sci. Catal.* **119**, 15 (1998).
28. Xu, J., and Froment, G., *AIChE J.* **35**, 88 (1989).
29. Bradford, M., and Vannice, M. A., *Catal. Rev. Sci. Eng.* **41**, 17 (1999).
30. Elmasides, C., Ioannides, T., and Verykios, X. E., *AIChE J.* **46**, 1260 (2000).